Radiocarbon, Vol 58, Nr 3, 2016, p 459–478 DOI:10.1017/RDC.2016.20

THREE YEARS OF $\Delta^{14}CO_2$ OBSERVATIONS FROM MAIZE LEAVES IN THE NETHERLANDS AND WESTERN EUROPE

D Bozhinova[1] • S W L Palstra[2] • M K van der Molen[1] • M C Krol[1,3] • H A J Meijer[2] • W Peters[1,2*]

[1]Wageningen University, Meteorology and Air Quality group, Droevendaalsesteeg 4, 6708 PB Wageningen, the Netherlands.
[2]University of Groningen, Centre for Isotope Research, Nijenborgh 4, 9747 AG Groningen, the Netherlands.
[3]Institute for Marine and Atmospheric Research Utrecht, Princetonplein 5, 3584 CC Utrecht, the Netherlands.

ABSTRACT. Atmospheric $\Delta^{14}CO_2$ measurements are useful to investigate the regional signals of anthropogenic CO_2 emissions, despite the currently scarce observational network for $\Delta^{14}CO_2$. Plant samples are an easily attainable alternative, which have been shown to work well as a qualitative measure of the atmospheric $\Delta^{14}CO_2$ signals integrated over the time a plant has grown. Here, we present the ^{14}C analysis results for 89 individual maize (*Zea mays*) plant samples from 51 different locations that were gathered in the Netherlands in the years 2010 to 2012, and from western Germany and France in 2012. We describe our sampling strategy and results, and include a comparison to a model simulation of the $\Delta^{14}CO_2$ that would be accumulated in each plant over a growing season. Our model simulates the $\Delta^{14}CO_2$ signatures in good agreement with observed plant samples, resulting in a root-mean-square deviation (RMSD) of 3.30‰. This value is comparable to the measurement uncertainty, but still relatively large (20–50%) compared to the total signal. It is also comparable to the spread in $\Delta^{14}CO_2$ values found across multiple plants from a single site, and to the spread found when averaging across larger regions. We nevertheless find that both measurements and model capture the large-scale (>100 km) regional $\Delta^{14}CO_2$ gradients, with significant observation-model correlations in all three countries in which we collected samples. The modeled plant results suggest that the largest gradients found in the Netherlands and Germany are associated with emissions from energy production and road traffic, while in France, the $^{14}CO_2$ enrichment from nuclear sources dominates in many samples. Overall, the required model-based interpretation of plant samples adds additional uncertainty to the already relatively large measurement uncertainty in $\Delta^{14}CO_2$, and we suggest that future fossil fuel monitoring efforts should prioritize other strategies such as direct atmospheric sampling of CO_2 and $\Delta^{14}CO_2$.

KEYWORDS: radiocarbon in plants, modern atmosphere, experimental, modeling, anthropogenic CO_2 emissions.

INTRODUCTION

Radiocarbon measurements have gained increasing attention in studies of the anthropogenic CO_2 emissions to the atmosphere (Levin et al. 2003; Ciais et al. 2010; Vogel et al. 2013; Turnbull et al. 2014b). However, even with the rapidly increasing number of observational sites around the globe that measure atmospheric $^{14}CO_2$ (Graven et al. 2012), the spatial resolution of the network limits the capacity to infer regional-scale CO_2 emissions. $\Delta^{14}CO_2$ measurement of annual plants can provide some additional information on a higher spatial scale and can be used in addition to semi-continuous measurements from the observational network. Plant samples have been shown previously to represent the atmospheric fossil fuel CO_2 mole fractions well (Hsueh et al. 2007; Riley et al. 2008; Bozhinova et al. 2013), but come with their own set of challenges.

Plants assimilate atmospheric CO_2 during their daily photosynthesis, so their $^{14}CO_2$ signature will be representative of only the daytime period. This period is usually characterized by well-mixed conditions and hence by smaller signals from anthropogenic CO_2 emissions. Additionally, growth limiting factors, such as available solar radiation, water, and nutrients, will modify the amount of assimilated CO_2. A plant sample will often differ from the atmospheric average due to the variable assimilation rate of the plant, and these growing conditions should be accounted for when interpreting such samples (Bozhinova et al. 2013). Furthermore, species-specific development differences also need to be considered, as samples are usually taken of a particular plant part (e.g. leaves), for which the assimilation period can

*Corresponding author. Email: wouter.peters@wur.nl.

differ (Bozhinova et al. 2013). In maize, for example, the leaves stop growing shortly after flowering, while the stems still accumulate carbohydrates for a bit longer, resulting in a different period for which these two parts of the same plant are representative of the atmospheric $\Delta^{14}CO_2$.

We present here an intensive regional sampling study conducted in 2010, 2011, and 2012 for western Europe, during which samples of maize (*Zea mays*) leaves were gathered from the Netherlands, Germany, and France. We draw inspiration from the similar studies for maize and grasses in North America (Hsueh et al. 2007; Riley et al. 2008) and an European study, which used samples of wine-ethanol to explore $\Delta^{14}CO_2$ from past years (Palstra et al. 2008). Nevertheless, this is the first attempt to map the atmospheric $\Delta^{14}CO_2$ spatial gradients from annual plants across Europe on such high spatial resolution. Our main motivation of this work is to report the ^{14}C analyses of our plant samples. We describe our complete sampling strategy and protocols, which also include the additional plant development information that was obtained from the cooperating farmers. This information allows us to evaluate the uncertainty associated with the assimilation rate and development rate of the sampled plants. In addition, we use a $\Delta^{14}CO_2$ modeling framework to further analyze the observations and to characterize the $\Delta^{14}CO_2$ gradients captured in them. This modeling framework was described previously in Bozhinova et al. (2014), with a few improvements that are explicitly described in our methods. We discuss the general use of plant samples for fossil fuel CO_2 emission verification and give recommendations for future sampling strategies.

MATERIALS AND METHODS

Experimental

In the period 2010–2012, we collected and analyzed 69 samples of maize leaves (*Zea mays*) from 35 individual locations in the Netherlands, most of which were sampled in both 2011 and 2012. In the last year, we also analyzed 20 samples collected from seven sites in the Ruhrgebiet area in Germany and nine sites in Lower Normandy and the Isle of France in France. These regions are strongly influenced by fossil fuel CO_2 and nuclear $^{14}CO_2$ emissions, respectively. A map with the sampled locations is shown in Figure 1, with the underlying anthropogenic CO_2 emission map (Institute for Energy Economics and the Rational Use of Energy, University Stuttgart, henceforth referred to as IER) to highlight the relatively emission-intensive regions. Additionally, in this figure we define four regions for the territory of the Netherlands, which we expect to show different characteristics. In order of expected fossil fuel emissions, these are Randstad, which is the densely populated industrialized region between Amsterdam, Rotterdam, and Utrecht; south Netherlands, which is the zone between Randstad and the Ruhrgebiet, a highly industrialized region in western Germany; central Netherlands, which covers the region between the Randstad and the north; and northern Netherlands, which is relatively rural and receives clean air with maritime characteristics from northwesterly winds.

We focused on maize as it is a crop that is available throughout most of Europe and particularly in the Netherlands. Additionally, due to the agricultural importance there is already a large expertise available in the scientific community with regard to its growth and development—both in observational and modeling studies. Using that modeling experience, previously discussed in Bozhinova et al. (2013), we chose to sample the leaves of the crop and sampled all leaves from each chosen plant. Theoretically, this would provide us with information for the atmospheric signals for a longer period than a single leaf. This is one of the differences between our work and a similar study executed in North America in the summer of 2004 (Hsueh et al. 2007), where most

https://doi.org/10.1017/RDC.2016.20 Published online by Cambridge University Press

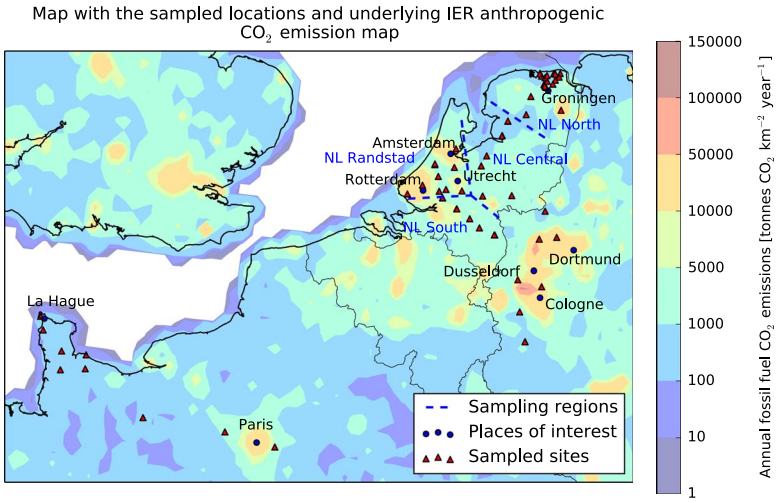

Figure 1 Overview of the sampled locations and the underlying fossil fuel CO_2 emissions map (annual estimate for 2012 based on the 2005 emission map developed by Institute for Energy Economics and the Rational Use of Energy, University Stuttgart). Dashed lines signify the borders of sampling regions later used in the presentation of our results.

of the samples represented a cross-section of the upper three leaves of each plant. Our sampling protocol also differed slightly and will be discussed in more detail later in this section.

In 2010, the study was focused on an area located in the northern part of the Groningen province in the Netherlands. Samples were taken with approximately 4 km between sampling sites in a triangular pattern between the city of Groningen, the Lutjewad observational station, and the Eemshaven, an industrial harbor area with several power plants. We used the modeling results for the average anthropogenic $^{14}CO_2$ and CO_2 mole fractions for 2008 presented in Bozhinova et al. (2014), and modified accordingly our sampling routes in 2011 and 2012 to try and capture the large $\Delta^{14}CO_2$ gradients expected between regions with higher or lower anthropogenic CO_2 emissions (illustrated in Figure 1). Thus, in these years the horizontal resolution between sampled locations increased to approximately 20 km and in some cases up to and exceeding 50 km. For the Netherlands, the sampled trajectories cover the distance between the Randstad and three different end points: eastwards towards the border with Germany, north towards the province of Groningen, and southeast towards the industrialized Rurhgebiet region in western Germany. In 2012, additional samples covering the area in Germany near the Rurhgebiet and samples covering a trajectory between La Hague and Paris in France were also taken.

To evaluate the role of the actual plant development in our interpretation of the gathered maize samples, additional information was obtained from the owners of each maize field. We asked for the dates when the field was sowed, when the emergence of the majority of the field was observed and the approximate date when the tassel (the pollen-producing flower at the top of the plant) had appeared, marking the flowering stage of the crop. We note that while the sowing was well known and the emergence was known to within a few days, the uncertainty associated with the flowering date is larger as this information was given as an approximate to within a week or two. The details about the dates obtained can be found in the online Supplementary Material (Table S1, General sample information).

https://doi.org/10.1017/RDC.2016.20 Published online by Cambridge University Press

In our sampling protocol, we always sampled plants at least 20–50 m away from the borders of the field. We picked plants that visibly appeared average compared to their neighbors and avoided sick and severely damaged plants. We gathered leaves from three plants for each sampled location. Those were not neighboring plants, but rather chosen within the same part of the field. For this study, we only analyzed all three individual plants obtained from sites #8, 9, 52, 62, 66, and 74, and otherwise analyzed only one plant sample per location. The rest of the material is archived for possible further investigation.

After sampling, the leaves were kept refrigerated until postsampling treatment. That included cleaning the leaves from dirt with water, cutting them into pieces, treating them with 1% solution of hydrochloric acid for 1 hr, and afterwards rinsing thoroughly with demineralized water until close to neutral pH value was reached. Afterwards, the samples were dried at 70°C for at least 48 hr. In 2010, the leaves were afterwards crushed manually into relatively small pieces, while in the latter years the samples were ground into powder using a laboratory grinder (Peppink 200AN, particle size <1 mm). Special care was taken to clean the grinder after each sample to avoid cross-contamination. The prepared samples were then sent for $^{14}CO_2$ analysis to the Centre for Isotope Research (CIO, University of Groningen, the Netherlands).

To analyze the maize samples for their ^{14}C content, these have first been combusted to CO_2. For the ^{14}C accelerator mass spectrometer (AMS) analysis, only a very small amount (<5 mg) of material is needed. We combusted 2 g of each sample in 2010 and extracted two subsamples to use for the further processing, while in 2011 and 2012, we combusted only 2×4.5 mg of each sample to obtain the two subsamples. This difference was a direct result of the grinding procedure and the reduced particle size in the sample material in the latter 2 years, which allowed us to obtain a more representative carbon mixture in a smaller sample before combustion.

In 2010, the samples were combusted using a handmade combustion system at the CIO. This system contains ovens with oxygen supply to combust the material to CO_2 and to oxidize formed CO to CO_2, several water-removing cryogenic traps, silver- and copper-containing ovens, and MnO_4 solution to remove sulfur- and nitrogen-containing components. The samples of 2011 and 2012 have been combusted with an elemental analyzer to CO_2 (Aerts-Bijma et al. 2001). Part of the CO_2 has been analyzed for $\delta^{13}C$ with an isotope mass ratio spectrometer and of the rest, for each obtained CO_2 sample, the two subsamples were graphitized to pure graphite (Aerts-Bijma et al. 1997, 2001). This graphite has been pressed into a target, on which we measured the carbon isotopes ^{12}C, ^{13}C, and ^{14}C using the ^{14}C-dedicated AMS at the CIO (van der Plicht et al. 2000). Both subsamples have been measured in the same AMS batch. Generally, an AMS batch has been measured twice, giving four ^{14}C measurement results for each maize sample. The AMS results were corrected for influences due to the preparation procedure using the results of AMS measurements of a graphitized ^{14}C-free CO_2 (Rommenhöller gas) sample or combusted anthracite. We should note that this is a minor correction for modern samples such as investigated in this study.

In Table A1 in the Appendix, we show the averaged results for each location and individual sampled plant. We report the $^{14}CO_2$ content of the sample relative to the modern standard as $\Delta^{14}CO_2$ [‰] following the conventions in the field for atmospheric CO_2 samples (Stuiver and Polach 1977; Mook and van der Plicht 1999). The number of analyses used for the reported average $\Delta^{14}CO_2$ results might differ in case there was a problem with the AMS measurement, or when additional analyses were performed. More detailed information can be found in the Online Supplementary Material (Table S2, ^{14}C analysis information).

https://doi.org/10.1017/RDC.2016.20 Published online by Cambridge University Press

Model Analysis

In our modeling study, we use the Weather Research and Forecast model (WRF-Chem version 3.2.1) to simulate the transport and mixing of CO_2 and $^{14}CO_2$ emissions as well as the weather conditions for a 6-month period, spanning April to September in 2010, 2011, and 2012. We use the daily weather information from the model together with the sowing dates reported by the farmers that contributed maize samples, as an input for a crop growth model to simulate the day-by-day crop growth for each sampling location. The crop model used is the Simple Universal CROp Simulator (SUCROS 2) that was used previously in Bozhinova et al. (2014). WRF-CHEM simulates mole fractions of atmospheric CO_2 and $^{14}CO_2$ to estimate the local $\Delta^{14}CO_2$ of the atmosphere for each hour of the growing season. When using the crop model as a weighted average function for the atmosphere (see Bozhinova et al. 2013), these models allow us to construct the $\Delta^{14}CO_2$ signature in different parts of the crop accumulated since the start of the growing period.

The model domain used in this study differs slightly from our work in Bozhinova et al. (2014). Our outer domain (121×116 grid points at 36 km horizontal resolution) now covers Europe and the surroundings of the Black Sea, while our second domain (199×193 at 12 km) spans western and central Europe. Here, we will show results only from the two domains with the highest horizontal resolution (4 km) that include the sampling sites covered in our campaigns in the Netherlands and western Germany and in 2012 also between Normandy and Paris (outlined with green and magenta in Figure 2). Our simulations use a time step of 30–180 s, but we use output of hourly intervals.

At every location in the WRF-CHEM domain (x,y,z), we simulate the CO_2 mole fraction changes over time (t) based on the following equation:

$$CO_{2sim}(x, y, z, t) = CO_{2bg}(x, y, z, t) + CO_{2ff}(x, y, z, t) + CO_{2p}(x, y, z, t) + CO_{2r}(x, y, z, t) \quad (1)$$

Here, the CO_2 mole fractions (in ppm) of different origin are indicated with subscripts as follows: fossil fuels (ff), biospheric photosynthesis (p), biospheric respiration (r), and background (bg). For our domain, the background term (CO_{2bg}) represents the atmospheric CO_2 levels affected by all processes not explicitly simulated for the WRF regional domain. This includes the initial conditions for CO_2, its inflow at the boundaries, as well as the influence of forest fires, ocean gas exchange, and stratospheric intrusions that occur outside our domain and are not simulated with WRF-CHEM. The CO_{2bg} varies over time and is modeled with the CarbonTracker Europe inverse modeling system (Peters et al. 2010).

The fossil fuel CO_2 emissions used in the model are based on the 2005 emission map provided at 5 (geographical) minutes horizontal resolution, developed by IER. A more elaborate description of the emissions sectoral, spatial, and temporal disaggregation is provided in Vogel et al. (2013). For the years simulated in this study, we have scaled the emissions from 2005 to 2010, 2011 and 2012 using the national and sectoral annual emission totals reported in the United Nations Framework Convention on Climate Change (UNFCCC). The emissions are vertically disaggregated and prescribed to the corresponding vertical layer in our WRF framework based on the average emission height for each model grid and emission sector as provided by IER. The fossil fuel inventory provides information as annual map and additional profiles for the different months, week days, and hours during the day that are category- and country-specific. Photosynthesis and respiration fluxes are calculated with the SIBCASA biosphere model (van der Velde et al. 2014) and downscaled with the same procedure as in Bozhinova et al. (2014).

https://doi.org/10.1017/RDC.2016.20 Published online by Cambridge University Press

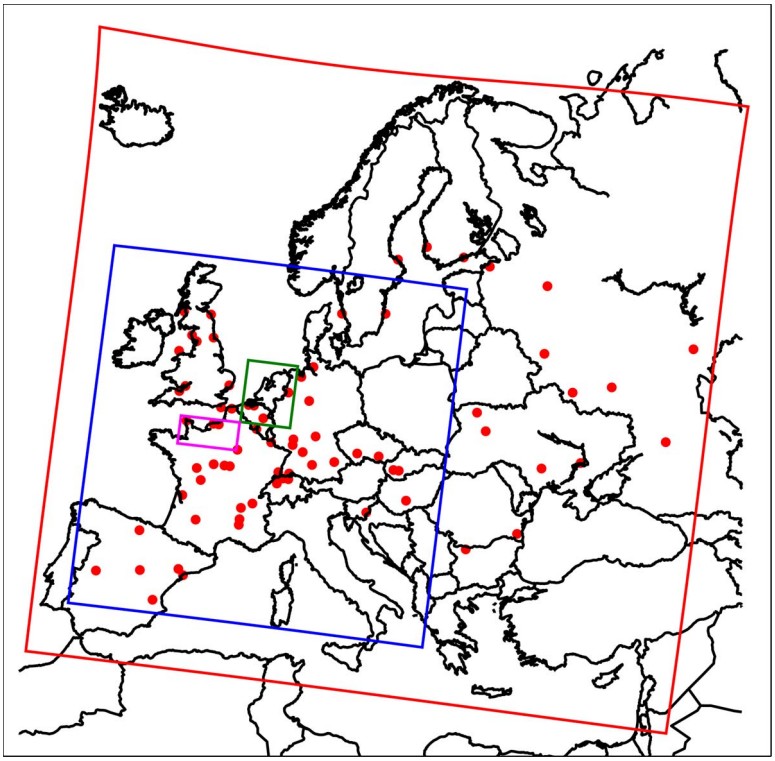

Figure 2 The four model domains used in WRF-Chem. Red indicates the outer borders of our simulation (36 × 36 km), while green and magenta indicate the borders of the domains used for our sample results (4 × 4 km). Red dots indicate the location of nuclear power plants or spent fuel reprocessing plants on our largest (indicated with red) domain (color references to online color version).

We use an equivalent expression to calculate the atmospheric $\Delta^{14}CO_2$ based on a combination of WRF-CHEM CO_2 and $^{14}CO_2$ tracers and their signatures:

$$\begin{aligned}(\Delta^{14}CO_2 \cdot CO_{2sim})(x,y,z,t) = {}& {}^{14}\Delta(^{14}CO^{dis}_{2bio} + {}^{14}CO^{dis}_{2o})(x,y,z,t) + \\ & {}^{14}\Delta(^{14}CO_{2n} + {}^{14}CO_{2c})(x,y,z,t) + \\ & \Delta_{bg}(t)(CO_{2bg} + CO_{2p} + CO_{2r})(x,y,z,t) + \\ & \Delta_{ff}CO_{2ff}(x,y,z,t) \end{aligned} \quad (2)$$

Here, we use three different Δ symbols: Δ_{ff}, Δ_{bg}, and $^{14}\Delta$ to provide signatures (in ‰) to simulated CO_2 (subscripts the same as in Equation 1) and $^{14}CO_2$ mole fractions of different origins. This includes the biospheric and oceanic disequilibrium, and both nuclear and cosmogenic sources as indicated by the symbols bio^{dis}, o^{dis}, n, and c, respectively, as discussed further below. $\Delta_{ff} = -1000‰$ as fossil fuel is entirely devoid of $^{14}CO_2$. $^{14}\Delta$ is the signature resulting from pure $^{14}CO_2$ emissions, i.e. a release of $^{14}CO_2$ without a concurrent flux of CO_2. It is calculated using the activity of a pure $^{14}CO_2$ (Bozhinova et al. 2014) sample calculated from

$$A_s = \frac{\lambda N_a}{m_{14C}} \quad (3)$$

where the Avogadro constant $N_a = 6.022 \times 10^{23}\,mol^{-1}$, $\lambda = 3.8534 \times 10^{-12}$ Bq is the decay rate of ^{14}C, and $m_{14C} = 14.0\,g\,mol^{-1}$ is the molar mass of the isotope. As there is no fractionation in a

https://doi.org/10.1017/RDC.2016.20 Published online by Cambridge University Press

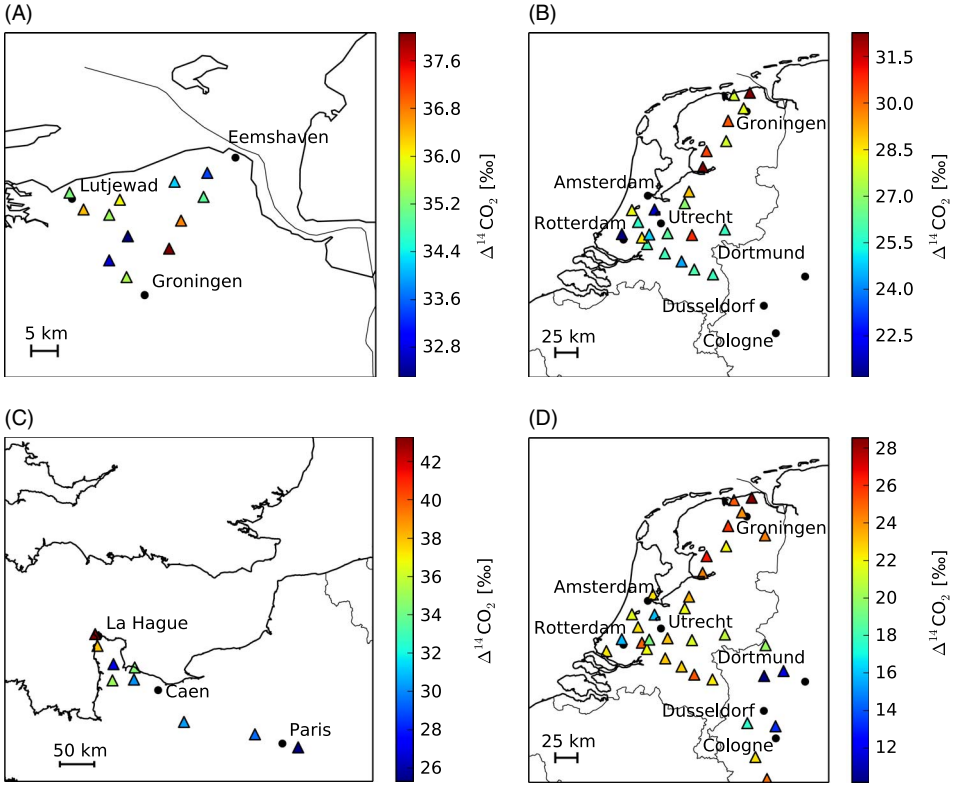

Figure 3 Sampling locations and ^{14}C analysis results for the 79 maize plant samples gathered in (A) 2010, (B) 2011, and (C and D) 2012. Plant samples gathered in urbanized and highly industrialized areas in the Netherlands, Germany, and France stand out with more depleted $\Delta^{14}CO_2$, while the ones gathered near La Hague show enrichment due to nuclear $^{14}CO_2$ influence. Note the different color scales in each plot, necessary to bring out the regional details among the large $\Delta^{14}CO_2$ spread across the four domains.

sample of pure ^{14}C, the calculation of the signature $\Delta^{14}CO_2$ (Stuiver and Polach 1977; Mook and van der Plicht 1999) can be simplified to the ratio between the activity of the sample and activity of the referenced standard $A_{ABS} = 0.226 \cdot \text{Bq g C}^{-1}$:

$$^{14}\Delta = A_s / A_{ABS} \cdot 1000[‰] \tag{4}$$

Finally, Δ_{bg} is the signature of air that is transported into the modeling domain and we assume this signature to be uniform in space across the domain, but to vary in time. CO_2 with this signature (bg, p, r) thus creates no additional spatial gradients in $\Delta^{14}CO_2$ across our domain. We take the value of Δ_{bg} from the time series of monthly observed $\Delta^{14}CO_2$ at the high alpine station Jungfraujoch [3450 m asl, Switzerland, data for the period courtesy to I Levin and S Hammer, Heidelberg University; partly published previously in Levin et al. (2013)]. This site is relatively close to our domain, yet far away from both the most intense nuclear and fossil source areas. An indication of its annual value is shown in Figure 4, but we note that through the daily plant growth patterns of each individual location in our domain, its expression in the final $\Delta^{14}CO_2$ differs for each plant. Our choice of Δ_{bg} (t) is elaborated later in our results and general discussion.

https://doi.org/10.1017/RDC.2016.20 Published online by Cambridge University Press

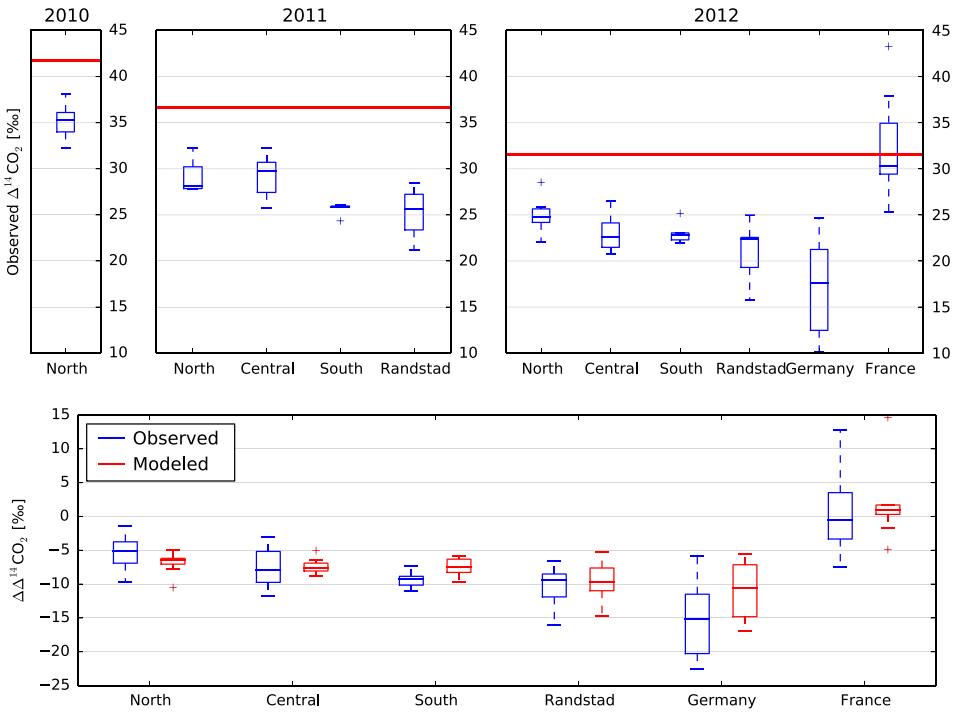

Figure 4 (Top) Sample results grouped by their respective region in the Netherlands, Germany, or France. The blue horizontal line shows the median, with the boxes representing the bottom 25% to the top 25% of data values, the whiskers are 1.5× this range, while values outside this range are shown as + signs. The May-June-July average of the Jungfraujoch $\Delta^{14}CO_2$ record is shown as a horizontal red line, as an indication of its typical average background value during each growing season. (Bottom) The same regionally grouped observations (blue) but now with the background contribution from Jungfraujoch removed (see Equation 2 and text), along with the simulated results (red) (color references to online color version).

The $^{14}CO_2$ emissions originating from nuclear power production are estimated from the International Atomic Energy Agency Power Reactor Information System (IAEA PRIS, available online at http://www.iaea.org/pris) by applying the method described in Graven and Gruber (2011) for the years of our study. The emissions for the active spent fuel reprocessing plants in La Hague, France, and Sellafied, UK, are based on the values officially reported by the companies operating the site for the monthly and annual gaseous releases (for La Hague - AREVA, www.areva.com; for Sellafield - Sellafield Ltd, www.sellafieldsites.com). Note that the current Sellafield emissions are far smaller (~50 times smaller) than the emissions from the site in La Hague, France. This is partly because 95% of the total ^{14}C release from Sellafield is liquid rather than gaseous releases (compared to only about 30% in La Hague), but also because the total ^{14}C release in Sellafield is smaller. All nuclear $\Delta^{14}CO_2$ emissions are prescribed at the vertical level in WRF that corresponds to the height of the emission stacks, where such information was available. In the cases where the emissions occur at surface level, these are introduced in the model in the lowest vertical layer. The nuclear emissions are available as annual totals and are averaged to their hourly values assuming continuous releases.

The disequilibrium fluxes result from older carbon dioxide that was typically $\Delta^{14}CO_2$ enriched when taken up by the biosphere or ocean, and now re-enters the atmosphere through plant respiration or ocean-atmosphere exchange. The monthly $^{14}CO_2$ fluxes (without the concurrent

https://doi.org/10.1017/RDC.2016.20 Published online by Cambridge University Press

Table 1 Information on the separate tracers simulated with WRF-CHEM in this study.

Tracer type	Term or code	Data source	Description
Background	CO_{2bg}	CarbonTracker	Background CO_2
Biosphere	CO_{2r}	SiBCASA	Ecosystem respiration of CO_2
Biosphere	CO_{2p}	SiBCASA	Photosynthetic uptake of CO_2
Biosphere	$^{14}CO^{dis}_{bio}$	Miller et al. (2012)	Biospheric disequilibrium of $^{14}CO_2$
Ocean	$^{14}CO^{dis}_{2o}$	Miller et al. (2012)	Oceanic disequilibrium of $^{14}CO_2$
Cosmogenic	$^{14}CO_{2c}$	Miller et al. (2012)	Cosmogenic production of $^{14}CO_2$
Fossil fuels	CO_{2ff}, SNAP 1	IER	Energy production sector
Fossil fuels	CO_{2ff}, SNAP 2	IER	Non-industrial combustion
Fossil fuels	CO_{2ff}, SNAP 3	IER	Combustion in manufacturing
Fossil fuels	CO_{2ff}, SNAP 4	IER	Production processes
Fossil fuels	CO_{2ff}, SNAP 7	IER	Road transportation
Fossil fuels	CO_{2ff}, rest	IER	Rest of the fossil fuel emissions
Nuclear	$^{14}CO_{2n}$, SFR	AREVA	Spent-fuel reprocessing emissions
Nuclear	$^{14}CO_{2n}$, PWR	IAEA	Pressurized water reactors
Nuclear	$^{14}CO_{2n}$, BWR	IAEA	Boiling water reactors
Nuclear	$^{14}CO_{2n}$, AGR	IAEA	Advanced gas-cooled reactors
Nuclear	$^{14}CO_{2n}$, MAG	IAEA	Magnox reactors
Nuclear	$^{14}CO_{2n}$, LWG	IAEA	Light-water-cooled reactors
Nuclear	$^{14}CO_{2n}$, rest	IAEA	Other nuclear reactors emissions

biospheric CO_2 exchange that we capture through CO_{2p} and CO_{2r}) for 2010 were taken from the study of Miller et al. (2012), and were interpolated to our finer model grid. These fluxes are calculated using biospheric and oceanic pulse response functions that account for the increase of the atmospheric $\Delta^{14}CO_2$ after the nuclear bomb tests in the 1950s and 60s and the turnover time of the carbon in the reservoirs. We use the 2010 fluxes for all 3 years for the ocean disequilibrium flux. The biospheric disequilibrium flux, however, we scale with the instantaneous temperature, which will result in this flux scaling with the ecosystem respiration of each year (Bozhinova et al. 2014).

The peak of cosmogenic production is located above the top of our model domain (50 hPa), and is inversely proportional to the solar activity. In 2010, the solar activity was at its minimum in the 11-yr solar cycle and the cosmogenic production was at its maximum. Our flux data (Miller et al. 2012) was available only for the year 2010 and we have used it also for the subsequent years, keeping in mind that the actual cosmogenic production following 2010 is likely smaller than what we have modeled. The disequilibrium fluxes and cosmogenic production are available as monthly averages and are also averaged to their hourly values before supplied to the WRF model. The list of all flux components (each presented by one WRF-CHEM model tracer) that we simulated in the equations is given in Table 1.

RESULTS

Our ^{14}C analysis of the plants from 51 locations sampled over 3 years are summarized in Table A1. In 2012, the statistics on the repeated analyses for many samples reduce the estimated error on the mean down to ~1.4‰. However, systematic errors during the measurement procedure cannot be eliminated with averaging over multiple analyses, and a more realistic lower limit for the measurement uncertainty on our samples is ~1.8‰. We evaluated the differences in $\Delta^{14}CO_2$ between plant samples that came from a single field for a subset of six locations (samples #8, 9, 58, 62, 64, and 74 in Table A1) and found that the variations between plants

https://doi.org/10.1017/RDC.2016.20 Published online by Cambridge University Press

from one sampling location are ±1.4–2.6‰. This is thus of comparable magnitude or slightly larger than the analytical uncertainty on the individual samples and presents a lower limit of interpretability to this sampling strategy. We note that the large spread across plants from site #74 (Normandy, France) is caused by a combination of samples #74.1 and #74.2 and thus not an artifact in a single plant. This site therefore incurs a very large spread between individual plants (±6.7‰), for which an explanation is lacking.

A view over the spatial domain shows that our measurements identify urbanized or industrialized areas by their considerably depleted $\Delta^{14}CO_2$ signature, as well as areas where nuclear $^{14}CO_2$ is significantly enriching the atmosphere. The separation between samples from different regions is visualized in Figure 3, where we note the different color scales on the different maps and different years. Our study is among the first to characterize the atmospheric $\Delta^{14}CO_2$ through annual plants in Europe at this scale, and our results show expected patterns between background and polluted areas similar to ones observed by Palstra et al. (2008) in wine ethanol, or by Riley et al. (2008) for California, or across the USA by Hsueh et al. (2007). We next group the samples from the Netherlands into four distinct regions, namely North, Central, South, and Randstad (previously indicated in Figure 1), and additionally group the samples from Germany and France.

We find differences between these larger regions that are consistent between the years. Figure 4A shows these regional gradients on top of the continuing decrease of atmospheric $\Delta^{14}CO_2$ of approximately –5‰/yr. This is best seen in our plant samples for the three consecutive years for the North region.The samples from 2011 and 2012 show a gradient from the cleaner (North) to the most polluted (Randstad) region in the Netherlands, and a further depletion towards the German Ruhr-area. Despite the large scatter between individual sampling locations, this behavior is consistent in the regional means for the 2 years. The annual downward trend is clearly an important component of an analysis that spans multiple years like ours, even more so because its magnitude is comparable to the largest gradients within the Netherlands. We note however that this annual depletion is not the same across several European atmospheric monitoring sites, and the choice of Δ_{bg} (t) in Equation 2 thus has an impact on the analysis of fossil-fuel-derived gradients that we are interested in, as we discuss further in the following section.

When we use the Jungfraujoch timeseries as Δ_{bg} (t) and the model for the plant growth for all samples, we can normalize across the years and regions and inspect relative gradients in Figure 4B. The median gradients within the Netherlands are typically small, and spatial gradients in $\Delta^{14}CO_2$ observed in the northern regions of the Netherlands were similar to the analytical uncertainty (~2.0‰) and within-field uncertainty (~2.5‰). The gradient between the most polluted Randstad samples and those in the North sometimes exceed this value though, and even larger gradients are found towards the German Ruhr area. Over distances of several hundreds of km, the urban centers thus stand out over more rural background sites, and so do the enriched locations in France. We note that the typical spread across multiple samples from the same region (the within-region variability) can also be close to 3‰ (indicated by the 25–75 percentile of the boxes in the most frequently sampled regions in the Netherlands), which is close to the within-field variability and the measurement uncertainty. Considering multiple samples from one region thus does not necessarily improve the signal-to-noise of the plant sampling method.

We next turn to our model to further analyze the gradients in the observed $\Delta^{14}CO_2$ between years and regions. Looking at the regionally aggregated model results in Figure 4 we see that our model underestimates this within-region variability, as well as the magnitude of the $\Delta^{14}CO_2$

https://doi.org/10.1017/RDC.2016.20 Published online by Cambridge University Press

gradient from the Netherlands to the German Ruhr area. It captures the median Randstad $\Delta^{14}CO_2$ depletion well though, and also reproduced the typical low fossil fuel regime and even enrichment in the samples from France. When considering the individual samples in Figure 5, we find that our model results correlate well ($r = 0.82$) with the observed values, especially when considering the analytical uncertainty of our plant samples of 1.8‰ to 3.0‰. In panel A, the model-to-observation root-mean-square difference (RMSD) is 3.91‰, when we exclude the largest positive value (La Hague sample of 43‰, but at modeled value of +235‰ falling outside the y scale shown on the figure). In Panel B, we have again used the Jungfraujoch monthly time series to normalize our sample population to a single European background. Panel B thus emphasizes European-scale fossil fuel gradients more, and year-to-year atmospheric $\Delta^{14}CO_2$ depletion as well as growing-season induced gradients less. This causes a clustering of the values closer to the 5–10‰ range and a smaller correlation coefficient ($r = 0.75$), as the correlation was partly driven by the model capturing the observed annual decrease through Δ_{bg}. However, the mismatch also becomes smaller as the RMSD is 3.30‰ (with the same model outlier excluded), and we find that the number of modeled sites that lie outside 6‰ of the observations (>2 × the within-region variability) decreases from 12 (approximately 15% of all our samples) to only 6 sites (less than 8% of all samples).

We note that the largest mismatches occur for the most depleted (and partly also most enriched) samples, which in turn causes the slope of the model-observation fit to be far away from the 1.0 line for which we aim. This mismatch, like the regional view in Figure 4B, points to an underestimate of the modeled fossil fuel $\Delta^{14}CO_2$ in the atmosphere in the German Ruhr area, which we ascribe to the large contribution of energy production and industrial processes to the observed $\Delta^{14}CO_2$ in plants. These emissions come from stacks, but such point sources are not well-represented in the 4-km modeling grid of WRF-CHEM, and we find that the simulated $\Delta^{14}CO_2$ in this area decreases with increasing model resolution due to the area averaging of such point source

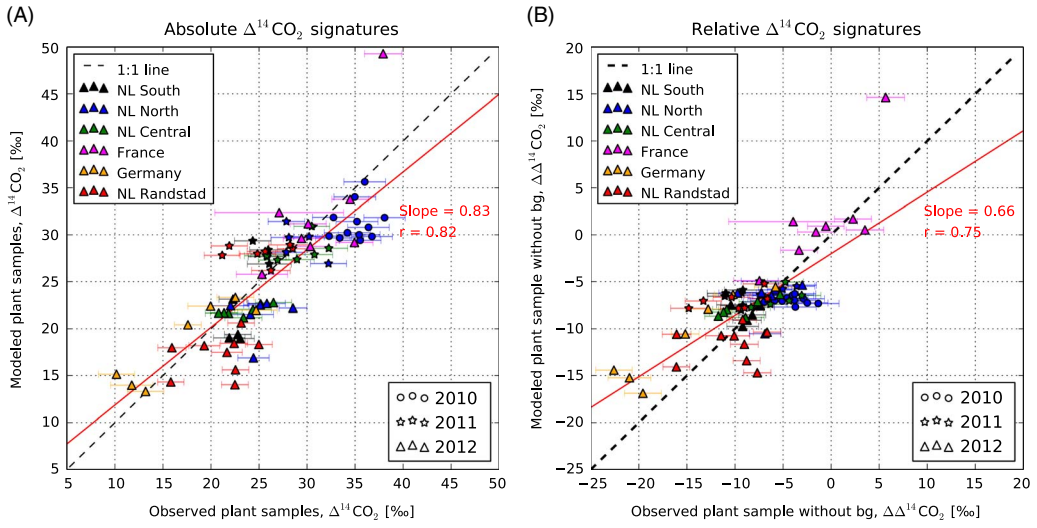

Figure 5 Comparison between modeled and observed plant samples for the different years and regions. In panel (A), we show the absolute signatures and here the modeled values were obtained by using observed $\Delta^{14}CO_2$ at Jungfraujoch as a background (Δ_{bg}). This is in contrast to panel (B) where we show the relative signatures and where the Jungfraujoch Δ_{bg} averaged over the period of plant growth is subtracted from each observed plant sample. In both panels, the result for the location of La Hague is outside the scale (+235‰ modeled value, +43‰ observed), and not included in the estimation of the linear regression of the data.

https://doi.org/10.1017/RDC.2016.20 Published online by Cambridge University Press

emissions on a grid. A specific plume model for these emissions would likely better capture their local contribution to plant samples, but this was not yet attempted in this study.

Within the different regions in our study, we find better model correspondence when we group the observations to the larger areas of Figure 4. Significant model-observation correlations were found in Germany ($r = 0.93$, $n = 7$, $p = 0.002$, slope = 0.69), France ($r = 0.78$, $n = 9$, $p = 0.01$, slope = 8.99), and with much smaller, but still significant numbers for the whole Netherlands ($r = 0.44$, $n = 59$, $p = 0.0004$, slope = 0.29) and the Randstad-Central-North trajectory ($r = 0.50$, $n = 49$, $p = 0.0002$, slope = 0.33). These results shows that the model captures such larger-scale gradients, but tests on an even smaller scale did not reveal significant correlations in almost all of the individual regions in the Netherlands. The only exception (the Central region, $r = 0.81$, $n = 12$, $p = 0.002$, slope = 0.3) is explained by the magnitude of the gradient, which is large over a relatively small domain as this region is situated between the polluted Randstad and cleaner North regions. With this note in mind, we will inspect the individual samples within each region and what is causing the observed and modeled gradients there.

According to our model results, the plant $\Delta^{14}CO_2$ depletion in the Netherlands and Germany is driven mainly by three categories of fossil fuel emissions: energy production, road traffic, and production processes. However, some enrichment from nuclear $^{14}CO_2$ and biospheric disequilibrium is present throughout all samples. Figure 6 shows the simulated composition of the $\Delta^{14}CO_2$ signature in maize leaves for each of our samples. Given the size of the gradients within a region it is clear that verifying the emissions from a locally dominant fossil fuel category (e.g. road traffic) will not be possible with plant samples. Furthermore, in most of France the enrichment due to nuclear $\Delta^{14}CO_2$ (especially from the spent-fuel reprocessing plant in La Hague) is so large that fossil fuel monitoring through $\Delta^{14}CO_2$ in plants will not be feasible. Near Paris (#78), the ratio between nuclear and fossil fuel influences is more favorable for such observations, but it will require careful evaluation of the nuclear $^{14}CO_2$ that is advected to the area. The modeled plant samples for our simulation domain seem to be influenced only very little by the $^{14}CO_2$ emissions from other types of nuclear sources, which is partly because the reactors with highest emissions are in the UK and not on mainland Europe.

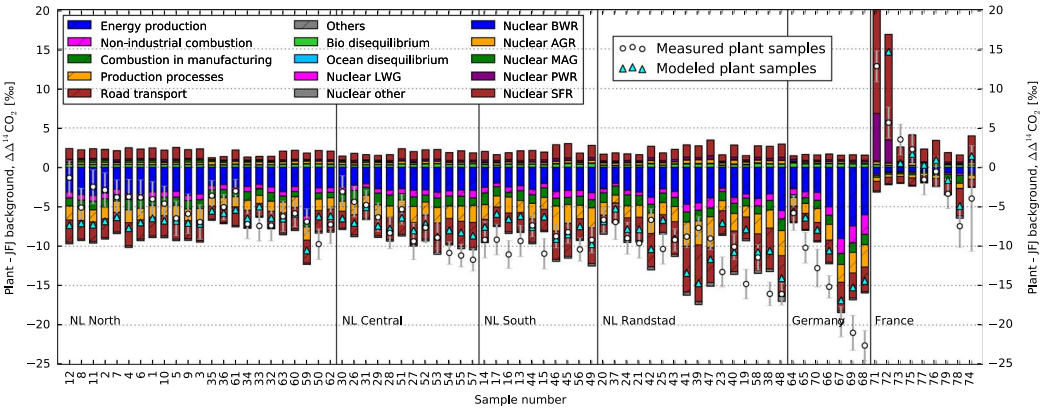

Figure 6 Model analysis of the additional enriching or depleting influences for each sampled location and year, where the sum of all contributions indicates the modeled plant samples. The small but consistent nuclear enrichment is found throughout the Netherlands in all years. Its effects are diminished for Germany, but greatly increased for France, where the ratio between nuclear to fossil fuel influence is strongly reversed. With the exception of France, the strongest signals are connected with the energy production, followed by road transport.

https://doi.org/10.1017/RDC.2016.20 Published online by Cambridge University Press

DISCUSSION

The choice of background site for the atmospheric $\Delta^{14}CO_2$ (Δ_{bg}) plays a minor role in the interpretation of our results. In Equations 1 and 2, we describe a framework in which air masses with initial CO_2 content of CO_{2bg} and $\Delta^{14}CO_2$ signature of Δ_{bg} travel through the domain and are influenced by the various local CO_2 and $^{14}CO_2$ sources to create the total simulated $\Delta^{14}CO_2$. We have confirmed that for the location Jungfraujoch, the modeled contribution to $\Delta^{14}CO_2$ from local sources is only –0.75‰ and this is thus indeed a relatively clean site in Europe. Moreover, we typically only evaluate simulated gradients in total $\Delta^{14}CO_2$ with this background subtracted from all samples (although filtered through the averaging kernel of each plant) such that its absolute value is of minor importance. Since we exclude the same background in both the simulated and measured values in our results, there is little chance of creating "false" gradients across our sites through this procedure. We chose to use the monthly mean observations from the site Jungfraujoch as this Δ_{bg} time series, as they were available for all 3 years of our study, and were most consistent with the observed annual decrease in the plant samples from our "clean" North region in the Netherlands. Choosing a site with a different decline in these 3 years such as for example Schauinsland would result in a different absolute magnitude of the $\Delta^{14}CO_2$ gradient, because Schauinsland shows very little $\Delta^{14}CO_2$ decline between 2010 and 2011, which might be due to changes in the local, or larger-scale influences at this site. However, we stress it would not change the overall site-to-site gradients presented in the results, nor the model-observation comparison.

Alternatively, we could have subtracted a local background $\Delta^{14}CO_2$ value that was taken specifically close to each site we sampled. In that approach, the only gradients would be caused by local emissions, which would be preferable for the interpretation of fossil fuel emissions. For a single instantaneous measurement, this would require obtaining Δ_{bg} upwind from the sampling location. However, for integrated air and plant samples the upwind region will vary throughout the sampling period. This is why previous studies preferred to use instead "clean-air" samples from approximately the same time as the samples, preferably from high-altitude sites that would be close proxies for the free tropospheric air (Turnbull et al. 2009). Because we lack good regional background samples for each site, we also adopted this strategy.

In terms of plant growth, size of the region sampled, regional $\Delta^{14}CO_2$ background, and the relative importance of the nuclear $^{14}CO_2$ emissions in the region, the samples from France differ most significantly from all others. With the exception of the two samples closest to the tip of Normandy (#71, 72), the observed samples are represented well by the model, as shown in Figure 5. Sample #71 and #72 are taken close to the spent fuel reprocessing plant (SFRP) in La Hague and show enrichment in their $\Delta^{14}CO_2$ signature in both model and observations, but the modeled results overpredict the observations quite considerably in the case of sample #71 (200+‰ modeled vs. 43‰ observed, outside the scale in all figures). Our observations are consistent with other plant and air measurements from this area. In a study conducted for the period 1997–1999, Fontugne et al. (2004) found similar and even more enriched $\Delta^{14}CO_2$ signatures in furze (flowering plants in the *Fabaceae* family), with large variability between neighboring samples on a spatial resolution of less than a kilometer. This indicates that to resolve the plume close to the source, our model would need a very fine resolution to capture the processes that currently occur at subgrid scale. The current domain resolution of 4×4 km is too coarse to capture the gradients created by the nuclear point source of La Hague's SFRP in the grid cells immediately surrounding it. Furthermore, we should note that in reality the temporal emission pattern from this site is not continuous as implemented in the model, but emissions occur about 10 to 15 times a day with each release lasting for 30 to 40 min. Since we compare with observations from plants, which integrate signals over a larger period, this difference will

https://doi.org/10.1017/RDC.2016.20 Published online by Cambridge University Press

have relatively small effect, but it will be more important if comparing to observations with higher temporal resolution.

In this work, we included several terms in the simulation of atmospheric $^{14}CO_2$ budget that were identified but not included in our previous study (Bozhinova et al. 2014), and we will first reflect on their possible influence on the plant samples we gathered. Our results show that in our domain the biospheric disequilibrium should be taken into account as its total contribution in our modeled plant samples varied up to 0.5‰ (Figure 6), while the influence of the ocean disequilibrium is negligible. These terms were considerably larger in previous decades and will continue to shrink in the future as the atmosphere-biosphere-ocean $\Delta^{14}CO_2$ equilibrates the excess ^{14}C that was produced in the atmosphere during the atmospheric bomb tests in the last century (Levin et al. 2010). The influence of cosmogenic production was at least 1000 times smaller than the biospheric disequilibrium. This was not only because the major part of the stratosphere is above the top of our model, as we found similarly small values in a test simulation where we distributed cosmogenic $\Delta^{14}CO_2$ production linearly with the pressure. This is consistent with the study of Turnbull et al. (2009), which showed that cosmogenic production has a significant influence only for the $\Delta^{14}CO_2$ observations obtained above 7000 m altitude. We find that only the spent nuclear fuel reactors in Europe significantly impacted the samples we collected, but this can be different for other samples across Europe.

We evaluated the uncertainty in our modeled plant results that is introduced when the modeled plant development differs from the observed. For this purpose, we used the additional developmental dates provided by our cooperating farmers (Table S1 in the online Supplementary Material) to vary the day of emergence and recalculate the plant signature depending on if the flowering date (where available) was modeled well by our plant growth model or not. The resulting differences to the signatures presented in the Results section can be considered an evaluation of the plant growth modeling error. The errors exceeded an absolute value of 1‰ for 15 (<20%) of our samples, with only 8 (~10%) of all cases exceeding 2‰. We should note that this is not the total model uncertainty, which in the case of atmospheric transport modeling is more difficult to estimate, but its size is already comparable to the intrinsic measurement uncertainty of our observations. A same argument can be made for the within-field variations in $\Delta^{14}CO_2$ that can be expected when picking several leaves from plants in one field: analysis of more than 30 samples from six sites quantifies this error as 1.6–2.6‰, which will be difficult or at least costly to reduce in any plant sampling strategy.

Our results agree with previous plant sampling studies (Hsueh et al. 2007; Palstra et al. 2008; Riley et al. 2008) that revealed regional fossil fuel emission patterns, and we further develop the model interpretation of the observed plant samples. This new modeling framework, however, is still unable to reproduce the variability in observed $\Delta^{14}CO_2$ in the most polluted areas, which was also the case in the study by Riley et al. (2008). Plant samples can be useful for the investigation of point sources (Turnbull et al. 2014a), but not all studies yet try to quantify the effect of the variable plant growth and its effect on the $\Delta^{14}CO_2$ signature of the assimilated CO_2. An additional complication when dealing with perennial plants (Park et al. 2013; Sakurai et al. 2013; Baydoun et al. 2015) could be the re-allocation of carbon assimilated from previous seasons for the initialization and maintenance of the current season growth. Despite our assumption at the start of our study that plants would be representative of the $\Delta^{14}CO_2$ in air over a larger area, we still find that the influence from point sources such as power production (Germany samples) and nuclear sources (La Hague) affects samples at a local scale, not captured in our 4-km modeling framework. The density of sampling to separate such sources from a regional background, or from more diffuse sources, is thus considerable.

https://doi.org/10.1017/RDC.2016.20 Published online by Cambridge University Press

Finally, we address the general use of plant samples of $\Delta^{14}CO_2$ in monitoring strategies of fossil fuel emissions. Our study, like previous work, shows that plant sampling is a cost-effective method to determine spatial gradients in fossil fuel content of the air between heavily industrialized or urbanized areas and their surrounding rural environments. Quantitative interpretation of such gradients, however, is difficult due to (1) the nuclear emissions of $^{14}CO_2$, (2) the intrinsic difference between plant and air samples, (3) the limited measurement precision compared to the fossil fuel gradients, and (4) the need for a good background regional reference $\Delta^{14}CO_2$ value. We show in this work that detailed modeling of emissions and plant uptake patterns can overcome issue (1) and (2), but in our study issues (3) and (4) precluded strong conclusions on fossil fuel emissions. An improvement in measurement precision to less than 1‰ would improve the prospects for $\Delta^{14}CO_2$-based fossil fuel monitoring through annual plant substantially. Until then, regional plant sampling can only provide limited information where other observational infrastructure is not yet available, where typical gradients in atmospheric $\Delta^{14}CO_2$ are not yet known, or where regional gradients are expected to exceed the current measurement precision by a very large margin.

In our view, other monitoring strategies that include $\Delta^{14}CO_2$ hold better promise. For example, combining continuous CO_2 and CO observations with integrated weekly or biweekly observations of atmospheric $\Delta^{14}CO_2$ (Levin and Karstens 2007; van der Laan et al. 2010; Vogel et al. 2010, 2013) allows an estimate of the fossil fuel CO_2 addition on a high temporal resolution. Although this method also has its challenges related to the constancy of emission factors over time and space, the time series generated this way allow a better evaluation of relative emissions strengths and transport patterns across the domain of interest than integrated plant samples. In addition, a range of chemical species measured in flask samples can help identify the influence of some specific anthropogenic sources (Turnbull et al. 2011; Miller et al. 2012). The combination of these methods, their implementation in existing observational networks, and the expansion of the observational network should in our opinion therefore receive higher priority when designing a fossil fuel monitoring methodology.

CONCLUSIONS

We have presented 3 years of plant-sampled $\Delta^{14}CO_2$ observations obtained throughout the Netherlands, Germany, and France, which show the distinct influence of fossil fuel CO_2 and nuclear enrichment on the atmospheric $\Delta^{14}CO_2$ on the regional scale. We find measurable differences between various sampled regions; however, their true gradients are difficult to evaluate directly due to the large year-to-year decrease in the average atmospheric $\Delta^{14}CO_2$ and large inherent measurement uncertainty in the observations. Still, the modeled gradients are captured relatively well by plant samples. From six sites, we determined that plant samples incur an inherent uncertainty due to within-field variations of 1.6–2.5‰.

Simulations of these plant samples compare well with the observed deviation from the regional background values with RMSD = 3.30‰. Depending on the sampled location, this could be from 20% and up to 50% of the total anthropogenic signal. This deviation is comparable with the combined measurement uncertainty of the plant samples, which varies from 1.8‰ to 3.0‰. We found significant correlations in all large (>100 km) regions sampled in our campaigns, which indicates that on this scale our model captures the observations relatively well. On smaller scales, the model generally is not able to reproduce the measured variability, with the notable exception of the Central region of the Netherlands ($r = 0.81$). This region is located between the urbanized and industrialized region of Randstad and the much cleaner region in the north of the Netherlands with possibly the largest regional gradients in $\Delta^{14}CO_2$ in the country.

https://doi.org/10.1017/RDC.2016.20 Published online by Cambridge University Press

Our modeling results shows that depletion in our plant $\Delta^{14}CO_2$ samples are driven mainly by emissions by energy production, road traffic, and production processes. This largely differs for the samples obtained in France, where nuclear enrichment dominates over the fossil fuel signals. Nevertheless, given the size of the gradients within regions, plant samples cannot be used to target specific emission categories.

ACKNOWLEDGMENTS

This work is part of project (818.01.019), which is financed by the Netherlands Organisation for Scientific Research (NWO). Further partial support was available by NWO VIDI grant (864.08.012). We acknowledge the Institute for Energy Economics and the Rational Use of Energy (University of Stuttgart) for providing the anthropogenic CO_2 emissions maps, IAEA PRIS for the nuclear reactor information, and NCEP and ECMWF for the meteorological data. We thank Ingeborg Levin and Sammuel Hammer (University of Heidelberg, Germany) and Felix Vogel, Michel Ramonet, and Martina Schmidt (LSCE, France) for providing the atmospheric $\Delta^{14}CO_2$ observations for Europe, and the ICOS infrastructure and SNO-ICOS-FRANCE monitoring network, which were used to obtain these. We further want to thank the Centre of Isotope Research staff (University of Groningen) for their help and guidance through the sample postprocessing and ^{14}C analysis process. Last, but not least, we would like to thank all participating farmers for their patience and cooperation in obtaining the plant samples and all the relevant accompanying information.

SUPPLEMENTARY MATERIAL

To view supplementary material for this article, please visit http://dx.doi.org/10.1017/RDC.2016.20.

REFERENCES

Aerts-Bijma AT, Meijer HAJ, van der Plicht J. 1997. AMS sample handling in Groningen. *Nuclear Instruments and Methods in Physics Research B* 123(1–4):221–5.

Aerts-Bijma AT, van der Plicht J, Meijer HAJ. 2001. Automatic AMS sample combustion and CO_2 collection. *Radiocarbon* 43(2A):293–8.

Baydoun R, Samad OE, Nsouli B, Younes G. 2015. Measurement of radiocarbon content in leaves near a cement factory in Mount Lebanon. *Radiocarbon* 57(1):153–9.

Bozhinova D, Combe M, Palstra SWL, Meijer HAJ, Krol MC, Peters W. 2013. The importance of crop growth modeling to interpret the $\Delta^{14}CO_2$ signature of annual plants. *Global Biogeochemical Cycles* 27(3):792–803.

Bozhinova D, van der Molen MK, van der Velde IR, Krol MC, van der Laan S, Meijer HAJ, Peters W. 2014. Simulating the integrated summertime $\Delta^{14}CO_2$ signature from anthropogenic emissions over Western Europe. *Atmospheric Chemistry and Physics* 14:7273–90.

Ciais P, Paris JD, Marland G, Peylin P, Piao SL, Levin I, Pregger T, Scholz Y, Friedrich R, Rivier L, Houwelling S, Schulze ED. 2010. The European carbon balance. Part 1: fossil fuel emissions. *Global Change Biology* 16(5):1395–408.

Fontugne M, Maro D, Baron Y, Hatté C, Hebert D, Douville E. 2004. ^{14}C sources and distribution in the vicinity of La Hague nuclear reprocessing plant: Part I—terrestrial environment. *Radiocarbon* 46(2):827–30.

Graven HD, Gruber N. 2011. Continental-scale enrichment of atmospheric $^{14}CO_2$ from the nuclear power industry: potential impact on the estimation of fossil fuel-derived CO_2. *Atmospheric Chemistry and Physics* 11(12):339–49.

Graven HD, Guilderson TP, Keeling RF. 2012. Observations of radiocarbon in CO_2 at seven global sampling sites in the Scripps flask network: analysis of spatial gradients and seasonal cycles. *Journal of Geophysical Research: Atmospheres* 117(D2):D02303.

Hsueh DY, Krakauer NY, Randerson JT, Xu X, Trumbore SE, Southon JR. 2007. Regional patterns of radiocarbon and fossil fuel-derived CO_2 in surface air across North America. *Geophysical Research Letters* 34(2):L02816.

Levin I, Karstens U. 2007. Inferring high-resolution fossil fuel CO_2 records at continental sites from

combined $^{14}CO_2$ and CO observations. *Tellus* 59(2):245–50.

Levin I, Kromer B, Schmidt M, Sartorius H. 2003. A novel approach for independent budgeting of fossil fuel CO_2 over Europe by $^{14}CO_2$ observations. *Geophysical Research Letters* 30(23):2194.

Levin I, Naegler T, Kromer B, Diehl M, Francey RJ, Gomez-Pelaez AJ, Steele LP, Wagenbach D, Weller R, Worthy DE. 2010. Observations and modelling of the global distribution and long-term trend of atmospheric $^{14}CO_2$. *Tellus B* 62(1):26–46.

Levin I, Kromer B, Hammer S. 2013. Atmospheric $\Delta^{14}CO_2$ trend in Western European background air from 2000 to 2012. *Tellus B* 65:20092.

Miller JB, Lehman SJ, Montzka SA, Sweeney C, Miller BR, Karion A, Wolak C, Dlugokencky EJ, Southon J, Turnbull JC, Tans PP. 2012. Linking emissions of fossil fuel CO_2 and other anthropogenic trace gases using atmospheric $^{14}CO_2$. *Journal of Geophysical Research: Atmospheres* 117(D8):D08302.

Mook WG, van der Plicht J. 1999. Reporting ^{14}C activities and concentrations. *Radiocarbon* 41(3): 227–39.

Palstra SWL, Karstens U, Streurman H, Meijer HAJ. 2008. Wine ethanol ^{14}C as a tracer for fossil fuel CO_2 emissions in Europe: measurements and model comparison. *Journal of Geophysical Research: Atmospheres* 113:D21305.

Park J, Hong W, Park G, Sung K, Lee K, Kim Y, Kim J, Choi H, Kim G, Woo H. 2013. A comparison of distribution maps of $\Delta^{14}C$ of 2010 and 2011 in Korea. *Radiocarbon* 55(2–3):841–7.

Peters W, Krol MC, van der Werf GR, Houweling S, Jones CD, Hughes J, Schaefer K, Masarie KA, Jacobson AR, Miller JB, Cho CH, Ramonet M, Schmidt M, Ciattaglia L, Apadula F, Helta D, Meinhardt F, di Sarra AG, Piacentino S, Sferlazzo D, Aalto T, Hatakka J, Strom J, Haszpra L, Meijer HAJ, van der Laan S, Neubert REM, Jordan A, Rodo X, Morgui JA, Vermeulen AT, Popa E, Rozanski K, Zimnoch M, Manning AC, Leuenberger M, Uglietti C, Dolman AJ, Ciais P, Heimann M, Tans PP. 2010. Seven years of recent European net terrestrial carbon dioxide exchange constrained by atmospheric observations. *Global Change Biology* 16(14): 1317–37.

Riley W, Hsueh D, Randerson J, Fischer ML, Hatch JG, Pataki DE, Wang W, Goulden ML. 2008. Where do fossil fuel carbon dioxide emissions from California go? An analysis based on radiocarbon observations and an atmospheric transport model. *Journal of Geophysical Research: Biogeosciences* 113:G04002.

Sakurai H, Tokanai F, Kato K, Takahashi Y, Sato T, Kikuchi S, Inui E, Arai Y, Masuda K, Miyahara H, Mundia C, Tavera W. 2013. Latest ^{14}C concentrations of plant leaves at high altitudes in the Northern and Southern Hemispheres: vertical stability of local Suess effect. *Radiocarbon* 55(2–3):1573–9.

Stuiver M, Polach H. 1977. Discussion: reporting of ^{14}C data. *Radiocarbon* 19(3):355–63.

Turnbull J, Rayner P, Miller J, Naegler T, Ciais P, Cozic A. 2009. On the use of $^{14}CO_2$ as a tracer for fossil fuel CO_2: quantifying uncertainties using an atmospheric transport model. *Journal of Geophysical Research: Atmospheres* 114:D22302.

Turnbull J, Karion A, Fischer ML, Faloona I, Guilderson T, Lehman SJ, Miller BR, Miller JB, Montzka S, Sherwood T, Saripalli S, Sweeney C, Tans PP. 2011. Assessment of fossil fuel carbon dioxide and other anthropogenic trace gas emissions from airborne measurements over Sacramento, California in spring 2009. *Atmospheric Chemistry and Physics* 11:705–21.

Turnbull JC, Keller ED, Baisden T, Brailsford G, Bromley T, Norris M, Zondervan A. 2014a. Atmospheric measurement of point source fossil CO_2 emissions. *Atmospheric Chemistry and Physics* 14:5001–14.

Turnbull JC, Sweeney C, Karion A, Newberger T, Lehman SJ, Tans PP, Davis KJ, Lauvaux T, Miles NL, Richardson SJ, Cambaliza MO, Shepson PB, Gurney K, Patarasuk R, Razlivanov I. 2014b. Towards quantification and source sector identification of fossil fuel CO_2 emissions from an urban area: results from the INFLUX experiment. *Journal of Geophysical Research: Atmospheres* 120(1):292–312.

van der Laan S, Karstens U, Neubert REM, van der Laan-Luijkx IT, Meijer HAJ. 2010. Observation-based estimates of fossil fuel-derived CO_2 emissions in the Netherlands using ^{14}C, CO and ^{222}Radon. *Tellus B* 62(5):389–402.

van der Plicht J, Wijma S, Aerts-Bijma AT, Pertuisot MH, Meijer HAJ. 2000. Status report: the Groningen AMS facility. *Nuclear Instruments and Methods in Physics Research B* 172(1–4):58–65.

van der Velde IR, Miller JB, Schaefer K, van der Werf GR, Krol MC, Peters W. 2014. Terrestrial cycling of $^{13}CO_2$ by photosynthesis, respiration, and biomass burning in SiBCASA. *Biogeosciences* 11:6553–71.

Vogel F, Hammer S, Steinhof A, Kromer B, Levin I. 2010. Implication of weekly and diurnal ^{14}C calibration on hourly estimates of CO-based fossil fuel CO_2 at a moderately polluted site in southwestern Germany. *Tellus B* 62(5):512–20.

Vogel FR, Tiruchittampalam B, Theloke J, Kretschmer R, Gerbig C, Hammer S, Levin I. 2013. Can we evaluate a fine-grained emission model using high-resolution atmospheric transport modelling and regional fossil fuel CO_2 observations? *Tellus B* 65:18681.

https://doi.org/10.1017/RDC.2016.20 Published online by Cambridge University Press

APPENDIX

Table A1 The ^{14}C analysis results from each sampling location used in this study.[1] Here, $\Delta^{14}C$ is the weighted average and $\pm\Delta^{14}C$ refers to the error on this mean* for each location. Locations with repeat measurements (*r*) of a sample or multiple plants analyzed are indicated with tiered numbers. The "Nr of analyses" refers to the total number of subsamples analyzed and used for the random error across a sample, or across a site. For the complete results and other metadata from each sampling location, please see the online Supplementary Material.

Sample nr	Lat.	Lon.	Sampling date (day-month-year)	Average $\Delta^{14}C$[‰]	$\pm\Delta^{14}C$ [‰]	Nr of analyses
			Netherlands, 2010			
1	53.394	6.360	30-7-2010	35.2	2.2	4
2	53.365	6.399	3-8-2010	36.4	2.2	4
3	53.318	6.523	3-8-2010	32.3	2.2	4
4	53.248	6.517	3-8-2010	35.5	2.2	4
5	53.277	6.469	4-8-2010	32.8	2.2	4
6	53.355	6.471	4-8-2010	35.4	2.2	4
7	53.380	6.502	5-8-2010	36.0	2.2	4
8.1	53.409	6.657	5-8-2010	37.5	2.2	4
8.1r1	53.409	6.657	5-8-2010	34.0	1.5*	9
8.2	53.409	6.657	5-8-2010	32.9	1.5*	9
8.3	53.409	6.657	5-8-2010	32.2	1.5*	9
8.all	53.409	6.657	5-8-2010	34.2	2.4	5
9.1	53.423	6.750	5-8-2010	31.9	3.1	2
9.2	53.423	6.750	5-8-2010	37.7	2.2	4
9.2r1	53.423	6.750	5-8-2010	33.5	1.5*	9
9.2r2	53.423	6.750	5-8-2010	31.4	1.5*	9
9.3	53.423	6.750	5-8-2010	32.7	2.3	4
9.all	53.423	6.750	5-8-2010	33.4	2.5	5
10	53.382	6.739	5-8-2010	35.0	2.2	4
11	53.343	6.674	5-8-2010	36.8	2.1	4
12	53.295	6.638	5-8-2010	38.1	2.2	4
			Netherlands, 2011			
13	51.559	5.965	22-8-2011	25.8	2.0	4
14	51.610	5.660	22-8-2011	26.1	2.3	3
15	51.694	5.453	22-8-2011	24.4	1.9	4
16	51.777	5.180	22-8-2011	25.9	1.7*	5
17	51.872	4.888	30-8-2011	26.0	1.9	4
19	51.973	4.473	23-8-2011	21.2	1.9	4
20	51.938	4.803	23-8-2011	28.5	1.6*	6
21	52.098	4.739	24-8-2011	25.6	1.9	4
23	52.225	5.011	24-8-2011	21.9	1.9	4
24	51.983	5.225	25-8-2011	26.2	2.0	4
25	51.970	4.924	30-8-2011	24.8	1.9	4
26	51.963	5.626	30-8-2011	30.8	1.9	3
27	52.017	6.169	31-8-2011	25.8	2.3	3
28	52.289	5.511	31-8-2011	26.9	2.0	4
29	52.408	5.584	31-8-2011	29.0	1.8	5
30	52.656	5.816	1-9-2011	32.3	2.0	4
31	52.820	5.882	1-9-2011	30.5	1.9	4

https://doi.org/10.1017/RDC.2016.20 Published online by Cambridge University Press

Table A1: (*Continued*)

Sample nr	Lat.	Lon.	Sampling date (day-month-year)	Average $\Delta^{14}C$[‰]	$\pm\Delta^{14}C$ [‰]	Nr of analyses
32	52.920	6.213	1-9-2011	27.8	2.0	4
33	53.388	6.356	1-9-2011	27.9	1.9	4
34	53.249	6.516	2-9-2011	28.1	1.9	4
35	53.408	6.625	2-9-2011	32.2	1.9	4
36	53.125	6.251	15-9-2011	30.2	1.6*	4
37	52.219	4.637	15-9-2011	28.2	2.2	3
			Netherlands, 2012			
38	52.225	5.011	27-8-2012	15.9	1.5*	8
39	52.431	4.984	27-8-2012	22.5	1.4*	8
40	52.228	4.636	27-8-2012	21.7	1.6*	6
41	52.098	4.739	27-8-2012	22.6	1.4*	8
42	51.938	4.803	27-8-2012	25.0	1.4*	8
43	51.983	5.225	27-8-2012	23.1	1.4*	8
44	51.610	5.660	28-8-2012	25.2	1.4*	8
45	51.694	5.453	28-8-2012	22.8	1.4*	8
46	51.778	5.187	28-8-2012	23.0	1.5*	7
47	51.850	4.220	28-8-2012	22.4	1.4*	8
48	51.974	4.472	28-8-2012	15.8	1.4*	8
49	51.874	4.885	28-8-2012	21.9	1.6*	6
50	52.920	6.213	30-8-2012	22.0	1.9	4
51	52.820	5.883	30-8-2012	26.5	1.9	4
52	52.651	5.813	30-8-2012	24.4	1.9	4
53	52.408	5.584	30-8-2012	23.4	1.9	4
54	52.289	5.511	30-8-2012	21.8	1.4*	8
55	51.963	5.626	6-9-2012	21.4	1.4*	8
56	51.559	5.957	6-9-2012	22.3	1.5*	8
57	52.017	6.169	6-9-2012	20.8	1.4*	8
58.1	51.970	4.924	10-9-2012	17.8	1.4*	8
58.2	51.970	4.924	10-9-2012	19.1	1.8	6
58.3	51.970	4.924	10-9-2012	20.9	1.8	6
58.all	51.970	4.924	10-9-2012	19.3	1.6*	3
59	53.023	6.868	11-9-2012	24.4	1.6*	6
60	53.388	6.356	11-9-2012	25.1	1.7*	5
61	53.409	6.657	11-9-2012	28.5	1.5*	7
62.1	53.261	6.488	11-9-2012	21.3	1.4*	8
62.2	53.261	6.488	11-9-2012	25.5	1.9	4
62.3	53.261	6.488	11-9-2012	25.5	1.9	4
62.all	53.261	6.488	11-9-2012	24.1	2.4	3
63	53.125	6.251	11-9-2012	25.8	1.9	4
			Germany, 2012			
64	50.447	6.806	14-9-2012	24.7	2.2	3
65	50.764	6.631	14-9-2012	22.5	1.9	4
66.1	51.111	6.512	14-9-2012	18.0	1.9	4
66.2	51.111	6.512	14-9-2012	16.0	1.9	4
66.3	51.111	6.512	14-9-2012	18.8	1.9	4
66.all	51.111	6.512	14-9-2012	17.6	1.4*	3

https://doi.org/10.1017/RDC.2016.20 Published online by Cambridge University Press

Table A1: (*Continued*)

Sample nr	Lat.	Lon.	Sampling date (day-month-year)	Average $\Delta^{14}C$[‰]	$\pm\Delta^{14}C$ [‰]	Nr of analyses
67	51.073	6.967	14-9-2012	13.2	1.9	4
68	51.585	6.800	15-9-2012	10.2	1.9	4
69	51.631	7.120	15-9-2012	11.8	2.2	4
70	51.900	6.836	15-9-2012	20.0	2.4	4
			France, 2012			
71	49.680	− 1.911	3-9-2012	43.3	1.9	4
72	49.543	− 1.803	3-9-2012	37.9	1.9	4
73	49.163	− 1.331	3-9-2012	34.9	1.9	4
74.1	49.367	− 1.391	4-9-2012	19.6	2.2	3
74.2	49.367	− 1.391	4-9-2012	29.0	2.4	3
74.3	49.367	− 1.391	4-9-2012	32.6	1.9	4
74.all	49.367	− 1.391	4-9-2012	27.1	6.7	3
75	49.391	− 0.949	4-9-2012	34.5	1.9	4
76	49.239	− 0.905	4-9-2012	30.1	1.9	4
77	48.864	0.292	4-9-2012	30.3	1.9	4
78	48.848	2.682	5-9-2012	25.3	2.7	2
79	48.902	1.763	5-9-2012	29.4	1.9	4

[1]Samples from sites #18 and #22 are missing from this table as these were not analyzed due to lack of information from the farmers.

*This random error is lower than the 1.8‰ lower limit of our instrumental precision, which is independent of the number of analyzed samples.

https://doi.org/10.1017/RDC.2016.20 Published online by Cambridge University Press